Journal of Alloys and Compounds 947 (2023) 169514

Contents lists available at ScienceDirect

Journal of Alloys and Compounds

journal homepage: www.elsevier.com/locate/jalcom

Amorphous Ge-Se-S chalcogenide alloys via post plasma sulfurization of atomic layer deposition GeSe for ovonic threshold switch applications

Sukhwan Jun [a], Seunggi Seo [a,c], Seungwon Park [a], Tae Hyun Kim [a], Minkyu Lee [a], Seok Man Hong [b], Taehoon Kim [b], Seung-min Chung [a], Taeyoon Lee [a], Myoungsub Kim [b,*], Hyungjun Kim [a,*]

[a] School of Electrical and Electronic Engineering, Yonsei University, Seoul 03722, Republic of Korea
[b] SK Hynix, 2091, Gyeongchung-daero, Bubal-eup, Icheon-si, Gyeonggi-do, Republic of Korea
[c] Department of Chemical Engineering, Stanford University, Stanford, CA 94305, USA

A R T I C L E I N F O

Article history:
Received 21 December 2022
Received in revised form 23 February 2023
Accepted 2 March 2023
Available online 5 March 2023

Keywords:
Ge-Se-S
Ge-Se chalcogenide
Atomic layer deposition
Sulfurization
OTS selector

A B S T R A C T

For the future scaling of 3D cross-point (X-point) memory, it is necessary to implement atomic layer deposition (ALD) of chalcogenides for ovonic threshold switch (OTS) applications. We investigated ternary Ge-Se-S amorphous chalcogenide alloys based on ALD process, motivated by the expectation of low off-current and stable OTS behavior by partially replacing S in binary Ge-Se. Ge-Se-S alloys were synthesized by post-deposition sulfurization of ALD $GeSe_2$ thin films. Especially, we investigated the growth characteristics and film properties of ALD $GeSe_2$ using $HGeCl_3$ precursors with $Se(SiMe_3)_2$ together with density-functional theory (DFT) calculations. By changing the temperature and the low-temperature plasma sulfurization time, the compositions of 10-nm-thick Ge-Se-S thin films were controlled along the $GeSe_2$-Ge_2S pseudo-binary line in ternary phase diagram. It was confirmed that the $Ge_5Se_3S_2$ alloys maintained an amorphous phase and excellent step coverage, similar to ALD $GeSe_2$. Finally, we compared the OTS electrical characteristics of 10-nm-thick ALD $GeSe_2$ with $Ge_5Se_3S_2$ amorphous chalcogenide thin films in a mushroom-type device with a 50-nm bottom electrode. The novel $Ge_5Se_3S_2$ had a slightly larger threshold voltage (V_{th}) drift than $GeSe_2$ but exhibited the advantages of a higher threshold field, lower off-current, and smaller V_{th} fluctuation up to 10^6 cycles.

Data availability: The data that has been used is confidential.

1. Introduction

In the late 1960 s, Ovshinsky discovered that chalcogenide materials (such as sulfide, selenide, and telluride) have a switching effect, which is called ovonic threshold switching (OTS) [1]. After approximately 40 years, various two-terminal selectors, including OTS for cross-point (X-point) arrays, have been studied owing to the cost-efficiency and performance limitations of conventional memories and the need to introduce neuromorphic computing systems [2,3]. The OTS selector is considered as the most promising candidate for X-point arrays for 1S1R structures connected in series with resistive memory elements because the OTS selector has the advantages of a low leakage current, high on-current, low latency, and suitable threshold voltage. OTS with these advantages are the technology that has been applied to mass production [4] of such as PCRAM (phase change RAM), CBRAM (conductive bridge RAM), OXRAM (oxide-based resistive RAM), and STT-MRAM (spin-transfer torque magnetic RAM) [5–7].

Phase change memory (PCM) materials, for which Ge-Sb-Te (GST) is the typical example, should have a rapid and reversible transition between amorphous and crystalline phases. In contrast, OTS materials should maintain an amorphous phase even at high temperatures for extended periods, which is induced by continuous and repetitive Joule heating with electrical switching. Since OTS materials are glass formers with strong bonding, it is appropriate to contain lighter elements with shorter bond-length, such as Se and S, rather than Te [8]. Moreover, in Ge- or Si-based chalcogenide alloys, an increase in the optical bandgap can be expected to achieve a lower off-current, for which Se and S are better than Te [9–11].

Recently, various atomic layer deposition (ALD)-based processes have been reported for OTS applications aiming for vertical X-point

* Corresponding authors.
E-mail addresses: myoungsub.kim@sk.com (M. Kim), hyungjun@yonsei.ac.kr (H. Kim).

https://doi.org/10.1016/j.jallcom.2023.169514
0925-8388/

(VXP) three-dimensional (3D) structures with improved step-coverage and cost per bit [12]. The study of chalcogenide ALD for OTS applications started few years ago, mainly with binary Ge-Te and Ge-Se [13–17]. The ALD Ge-Te showed excellent step-coverage and electrical feasibility, but revealed limitations in low crystallization temperature and insufficient reliability characteristics for OTS applications. In the case of ALD Ge-Se, various research groups have studied OTS applications due to excellent thermal stability, and there have been many $GeSe_x$-based OTS studies with various elements to investigate the effect of incorporation of Sb, N, C, As, etc., improve, and control the performance for a selector [18–21]. For example, V. Adinolfi et al. have published a study of ternary ALD Ge-Se-Te in which the threshold voltage (V_{th}) increases and the leakage current decreases by including Se in ALD Ge-Te using the super-cycle ALD method of Ge-Te and Ge-Se [18]. However, no research based on Ge-Se-S alloy for OTS application has been reported although incorporating S into Ge-Se can lead to the better OTS performance owing to its shorter bonding length and higher optical bandgap than Se. Furthermore, there only have been ALD OTS studies containing the fundamental electrical characteristic analysis such as on/off current ratio, V_{th}, and endurance of resistance, even though extensive and in-depth studies of electrical characteristics such as V_{th} drift and V_{th} fluctuation are vital to prepare practical application and mass production of future 3D VXP memory.

In this study, we succeeded in synthesizing the novel ternary ALD Ge-Se-S alloy containing S of stronger bonding to ALD Ge-Se, revealing the advantages of OTS application of ternary Ge-Se-S devices. Here, we developed a two-step process of a novel Ge-Se-S alloy consisting of ALD $GeSe_2$ followed by post-sulfurization. Then, thin films were fabricated for 50-nm technology devices using ALD $GeSe_2$ and $Ge_5Se_3S_2$ chalcogenide alloy. We analyzed the preliminary DC characteristics, the fundamental first firing phenomenon, V_{th}, and leakage current characteristics for the first time. In addition, a reliability analysis of the V_{th} drift, V_{th} fluctuation, and endurance of the ALD $GeSe_2$ and $Ge_5Se_3S_2$ devices was performed. Furthermore, the device characteristics of a novel ALD-based $Ge_5Se_3S_2$ OTS material were compared with those of conventional ALD $GeSe_2$, and the advantages of high V_{th}, low leakage current, and reliability characteristics were extensively discussed.

2. Material and methods

2.1. DFT calculations

All DFT calculations were performed using the Gaussian 16 suite of programs [22]. All the geometries were optimized with Becke's three-parameter hybrid functional (B3LYP) [23,24]. For dispersion correction, Grimme's dispersion with Becke–Johnson damping (GD3BJ) was used [25,26]. For the DFT calculation, the Def2SVP basis set was used for Si and Ge, and Def2TZVP was used for H, C, and Cl. The LanL2DZ basis set with an effective core potential (ECP) was used for Se.

2.2. Sample preparation

The ALD of Ge-Se thin films and the post-sulfurization process were investigated using traveling waveform type equipment (SNTEK Co., LTD) using trichlorogermane ($HGeCl_3$), bis (trimethylsilyl) selenide ($Se(SiMe_3)_2$) precursors, and a hydrogen sulfate (H_2S) gas reactant. In the ALD process, a canister of the $HGeCl_3$ precursor with a high vapor pressure of approximately 100 Torr at 30 °C was used with a refrigerated water bath circulator (Jeio Tech, RW3–25) lowered to 3 °C. The $Se(SiMe_3)_2$ precursor was maintained at a vapor pressure of approximately 5 Torr at 40 °C using a heating tape on the canister. Ar purging was performed at 30 sccm using a mass flow controller (MFC). The base pressure of the ALD chamber was 25 mTorr, and the working pressure was set at ~1.5–2.0 Torr by adjusting a throttle valve. For sulfurization of the Ge-Se thin film, inductively coupled RF plasma was applied in a H_2S and H_2 gas atmosphere. Chamber heating and cooling was performed under Ar 50 sccm flow conditions, and inductively coupled RF plasma 150-W conditions were applied while flowing H_2S at 20 sccm and H_2 at 20 sccm, at the target sulfurization temperature, as shown in Fig. S1.

2.3. Film analysis and electrical measurements

The thickness of the thin film was measured using a model-validated spectroscopic ellipsometer (SE, Ellipso Technology, Elli-SE-F) and a scanning electron microscope (SEM, Hitachi, su-9000). Atomic composition and impurity analyses of the thin films were performed using Auger electron spectroscopy (AES, ULVAC, PHI-710), X-ray photoelectron spectroscopy (XPS, Thermo Fisher Scientific, K-Alpha), and focused ion beam transmission electron microscopy equipped with energy-dispersive spectroscopy (FIB-TEM/EDS, JEOL, JEM F-200). FIB-TEM was also used to confirm the step coverage of the ALD thin films. Atomic force microscopy (AFM, Bruker, Dimension ICON) was used to analyze surface roughness. The amorphous phase and optical bandgaps (E_g) of the thin films were determined using X-ray diffraction (XRD, Rigaku, SmartLab) and ultraviolet-visible near-infrared spectrophotometry (UV-NIR, Agilent, Cary 5000) measurements. For the OTS device, ALD Ge-Se and Ge-Se-S thin films were deposited on a patterned substrate, including a 50-nm-diameter TiN bottom electrode contact (BEC). Subsequently, an amorphous carbon layer (ACL) and Ru were deposited by sputtering, and the top electrode (TE) was patterned. The electrical characteristics were measured using a Keithley 4200A-SCS parameter analyzer with two source-measure units (4200-SMU), an ultrafast pulse measurement unit (4225-PMU), and two remote preamplifier/switch modules (4225-RPM).

3. Results and discussion

3.1. DFT calculations

To study the reaction between $HGeCl_3$ and $Se(SiMe_3)_2$ as the precursor and reactant, we investigated the coordinate diagram of the ALD reaction using DFT calculations, as shown in Fig. 1. As $HGeCl_3$ is known to be decomposed by the $GeCl_2$ + HCl reaction [17], the half-reactions of the ALD process were simulated by calculating

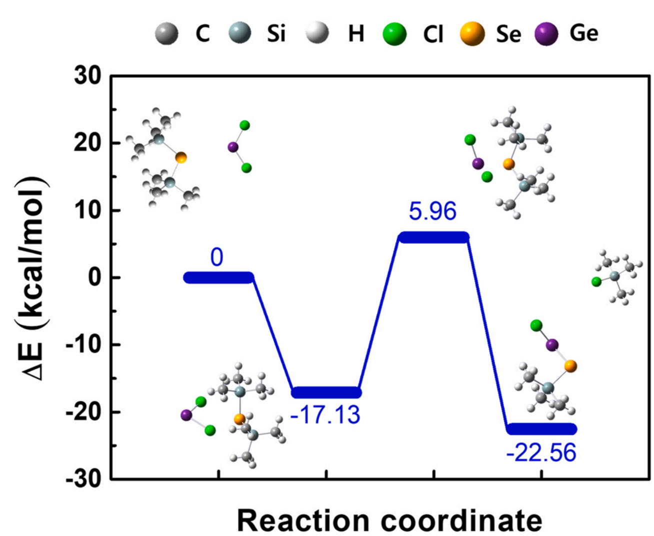

Fig. 1. Proposed reaction coordinate diagram between $HGeCl_3$ and $Se(SiMe_3)_2$ precursor.

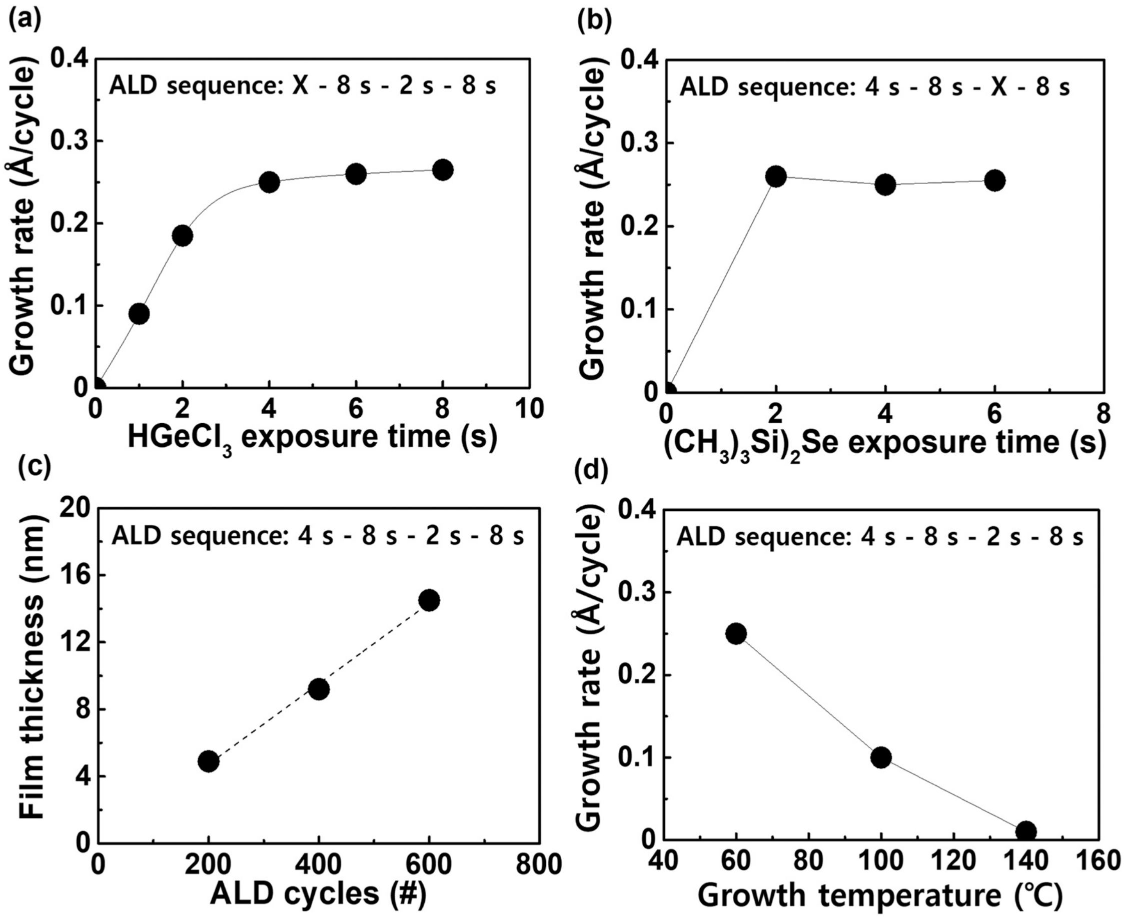

Fig. 2. Growth and self-limited saturation behavior of ALD at 60 °C using a $HGeCl_3$ and $Se(SiMe_3)_2$ precursor as a function of: (a) $HGeCl_3$ exposure time; (b) $Se(SiMe_3)_2$ exposure time; (c) Film thickness with various numbers of ALD cycles; (d) Growth temperature; (e) TEM image, TEM-EDS elemental mapping of Ge, Se and composition analysis of a 10-nm-thick ALD $GeSe_2$ thin film on a SiO_2 trench pattern wafer.

the ligand-exchange reactions of $GeCl_2$ with the $Se(SiMe_3)_2$, as shown below [27,28].

$$GeCl_2 + Se(SiMe_3)_2 \rightarrow ClGeSe(SiMe_3) + SiMe_3Cl$$

The adsorption energy of $Se(SiMe_3)_2$ and $GeCl_2$ is 17.13 kcal/mol with exothermicity. After physical adsorption, Cl atoms from $GeCl_2$ migrate to $Se(SiMe_3)_2$ with activation barriers of 23.09 kcal/mol. Finally, after Cl migration and desorption of the $SiMe_3Cl$ byproduct, the final structure of each reaction was changed to $ClGeSe(SiMe_3)$. The exothermicity for each reaction is 22.56 kcal/mol. In this result, it can be predicted that the ALD reaction of $HGeCl_3$ and $Se(SiMe_3)_2$ is a reasonable process on the physisorption energy, activation barrier, and chemisorption energy of the final state.

3.2. ALD growth characteristics of Ge-Se

Fig. 2 shows the growth characteristics of ALD Ge-Se thin films on SiO_2 substrates as a function of the $HGeCl_3$ and $Se(SiMe_3)_2$ precursor exposure time, number of ALD cycles, and growth temperature. Fig. 2(a–c) show the growth rate of self-limiting growth behavior with a GPC (growth per cycle) of 0.25 Å/cycle in the ALD sequence of Ge precursor (4 s); Ar purge (8 s); Se precursor (2 s); and Ar purge (8 s) at a growth temperature of 60 °C. Fig. 2(d) shows the change in the growth rate of the ALD Ge-Se thin films as a function of the growth temperature. It was observed that the growth rate of 0.25 Å/cycle at 60 °C decreased to 0.1 Å/cycle at 100 °C, whereas the growth observed at 140 °C was negligible. This result was similar to those of previous Ge-Se ALD studies, which discussed the desorption potential of volatile Se at elevated temperatures [14,16].

Fig. 2(e) shows cross-sectional FIB-TEM and EDS element (Ge, Se) mapping images of the 10-nm-thick ALD Ge-Se thin film, to evaluate the step coverage and quantitative elemental composition. The substrate used had a 12:1 aspect ratio with a width of 200 nm and a SiO_2 height of 2400 Å on the Si wafer. The step coverage, including top, side, and bottom, demonstrated the advantage of ALD, with excellent conformality of approximately 94 %. Fig. S2(a) shows the AES depth profile analyzed for the composition and impurities of the ALD Ge-Se thin film at a growth temperature of 60 °C. The composition of the ALD Ge-Se thin film was identified as $Ge_{0.32}Se_{0.68}$, except for approximately 4 % of oxygen and silicon impurities, which can be called the stoichiometric composition of $GeSe_2$. The atomic composition of the ALD $GeSe_2$ alloy was supported by the TEM-EDS analysis results in Fig. 2(e).

3.3. Composition control using post sulfurization

We performed a two-step post-sulfurization process to synthesize Ge-Se-S alloys based on $GeSe_2$ thin films with confirmed ALD behaviors. To control the composition of the Ge-Se-S alloys without crystallization from the ALD $GeSe_2$ amorphous thin films, the plasma sulfurization temperature was controlled between 100 and 300 °C for 30 min (Fig. S1). Fig. 3(a–c) show the XPS measurement results for the Ge 3d, Se 3d, and S 2p binding energies of the atomic composition change, depending on the plasma sulfurization temperature of the 30-nm-thick ALD $GeSe_2$ thin films. As the sulfurization

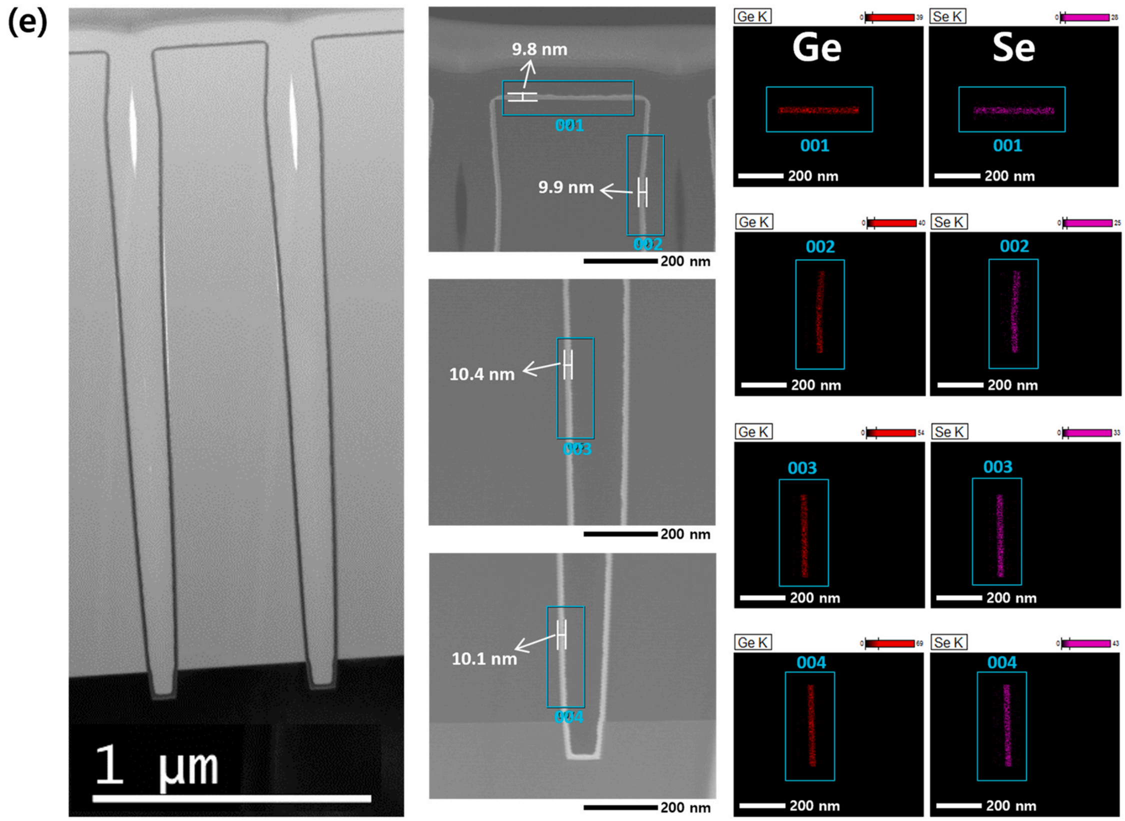

Position	Ge (atom%)	Se (atom%)
001	37.7	62.3
002	34	66
003	37.8	62.2
004	36.9	63.1

Fig. 2. (*continued*)

temperature increased, the peak corresponding to Ge 3d in Fig. 3(a) shifted from Ge-Se (~31.3 eV) to Ge-S (~30.5 eV), and these peak shifts mean composition change from Ge-Se to Ge-S which is attributed to decrease of Ge-Se peak intensity and increase of Ge-S peak intensity. In addition, Fig. 3(b, c) show that the peaks corresponding to Se 3d (~55.0 eV) and Se 3p (~160.9 eV) decreased; however, increase of S 2p (~162.5 eV) was clearly observed. In the plasma sulfurization process, it was confirmed that the Se atoms were spontaneously replaced by S atoms in the S-rich environment. [29] The AES depth profile analysis in Fig. S2 supports the compositional change of the ALD $GeSe_2$ thin film to Ge_x-Se_y-S_z in the depth direction without a significant change in impurities. Fig. 3(d) shows the composition-controlled results along the $GeSe_2$-Ge_2S pseudo-binary line by changing the temperature and time of the plasma sulfurization process in the Ge-Se-S ternary diagram. In particular, the low-temperature plasma sulfurization process revealed that the desorption of Se atoms was more dominant than the adsorption of S atoms from the results of the complete conversion of ALD $GeSe_2$ to the Ge_2S alloy. In addition, ALD $Ge_5Se_3S_2$ via post-plasma sulfurization was confirmed to have an amorphous phase by XRD measurements in Fig. S3. As shown in Fig. 3(e), from FIB-TEM and EDS analysis, it was shown that the ALD $Ge_5Se_3S_2$ alloy thin film synthesized through the 10-nm-thick ALD $GeSe_2$ and subsequent plasma sulfurization process (300 °C, 30 min) exhibited uniform atomic distribution and slight degradation of surface morphology at the top side of the trench, which can be attributed to damage by reactive H_2S plasma species such as proton.[30] To confirm the morphology degradation by the plasma process, the surface roughness RMS (root-mean-square) through AFM analysis was measured (Fig. S4). As a result, the surface roughness increased slightly from 1.01 to 2.04 nm compared to ALD $GeSe_2$, and this result is consistent with Fig. 3(e).

3.4. DC characteristics

ALD of binary $GeSe_2$ and ternary $Ge_5Se_3S_2$ amorphous chalcogenide alloys was studied in terms of their OTS electrical characteristics. Fig. 4(a) shows a schematic of the electrical measurement system, including the PMU with RPM for the reliability analysis, as well as the SMU for the basic DC test. Fig. 4(b) shows an FIB-TEM cross-sectional image of a mushroom-type OTS device with a 10-nm-thick OTS cell (ALD $GeSe_2$, $Ge_5Se_3S_2$)/intermediate electrode (ACL)/TE (Ru) structure on a 50-nm BEC (TiN). An ACL was applied as an intermediate electrode to improve device reliability and performance [31]. In addition, a 10-kΩ load resistor was included to minimize device degradation owing to the current overshoot in the V_{th} region. Fig. 4(c, d) show the DC I–V curves of the $GeSe_2$ and $Ge_5Se_3S_2$ devices measured at room temperature with a compliance current of 100 mA. The OTS devices exhibited the first firing behavior to initialize the amorphous chalcogenide cells and drive them to

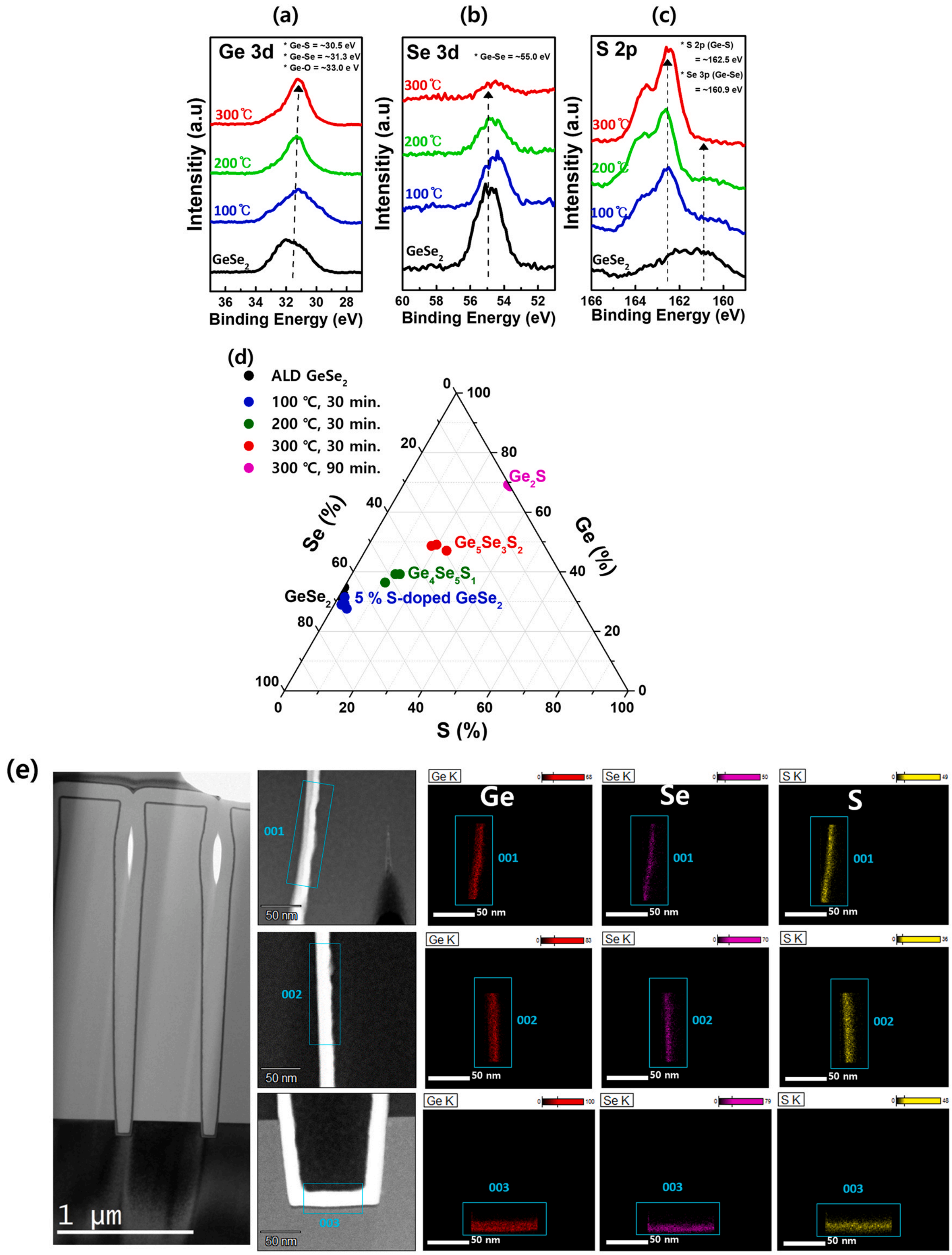

Position	Ge (atom%)	Se (atom%)	S (atom%)
001	54.0	24.8	21.2
002	55.7	25.2	19.1
003	55.2	26.0	18.8

Fig. 3. XPS spectra for (a) Ge 3d; (b) Se 3d; and (c) S 2p core levels of Ge-Se-S alloys through the plasma sulfurization temperature. (d) Ge-Se-S ternary diagram showing the composition-controlled alloys via the ALD $GeSe_2$ and post plasma sulfurization. (e) TEM image, TEM-EDS elemental mapping of Ge, Se, S and composition analysis of a 10-nm-thick ALD $Ge_5Se_3S_2$ thin film on a SiO_2 trench pattern wafer.

stationary behavior. The 10-nm-thick ALD $GeSe_2$ devices showed a median value of first firing voltage (V_{ff}) and threshold voltage (V_{th}) of 3.4 and 1.9 V, respectively. In contrast, the 10-nm-thick ALD $Ge_5Se_3S_2$ devices showed higher median values for V_{ff} and V_{th} of 4.3 and 3.2 V, respectively, compared to that of $GeSe_2$ devices. These changes of the electrical parameters can be related to E_g difference of

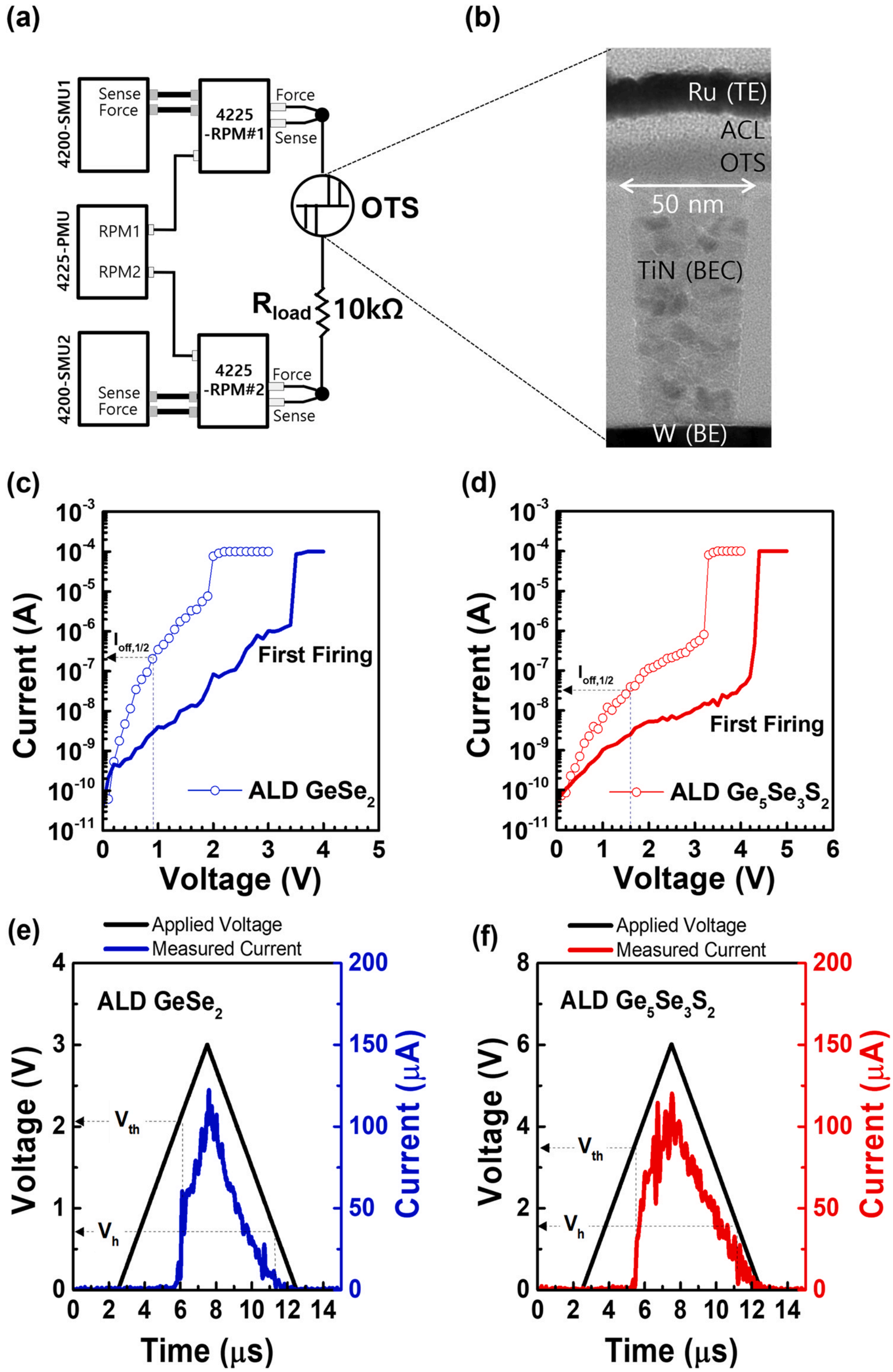

Fig. 4. OTS device characteristics of 10-nm-thick ALD $GeSe_2$ and $Ge_5Se_3S_2$ thin films. (a) Schematic of electrical measurement; (b) Cross-section FIB-TEM image of mushroom-type OTS device on a 50-nm BEC; (c, d) DC I–V curves; (e, f) Triangular pulsed I–V curves.

chalcogenide films, and the E_g of $GeSe_2$ and $Ge_5Se_3S_2$ will be compared later in this paper. Also, it is remarkable that V_{th} of $Ge_5S_3Se_2$ is higher than that of previously reported $(Ge_{0.6}Se_{0.4})_{0.78}Sb_{0.22}$, having same Ge and Se contents with $Ge_5Se_3S_2$ except for S, even though the thickness of $Ge_5Se_3S_2$ was much thinner than $(Ge_{0.6}Se_{0.4})_{0.78}Sb_{0.22}$ [32]. It can be also explained by higher E_g of $Ge_5Se_3S_2$ attributed to S incorporation as mentioned in introduction. ALD $Ge_5Se_3S_2$ with higher threshold field (E_{th}) characteristics has a very important scaling advantage in VXP architecture, where the thin film thickness directly affects chip size [9].

In addition, ALD $Ge_5Se_3S_2$ showed good off-leakage properties, which were significantly lower from ~200 to ~40 nA compared to ALD $GeSe_2$ based on the normalized off current at half V_{th} ($I_{off,1/2}$). Low leakage current is another significant key performance indicator for high-density implementation and scaling, because the low I_{off} characteristics of the OTS device can reduce the sneak current of the

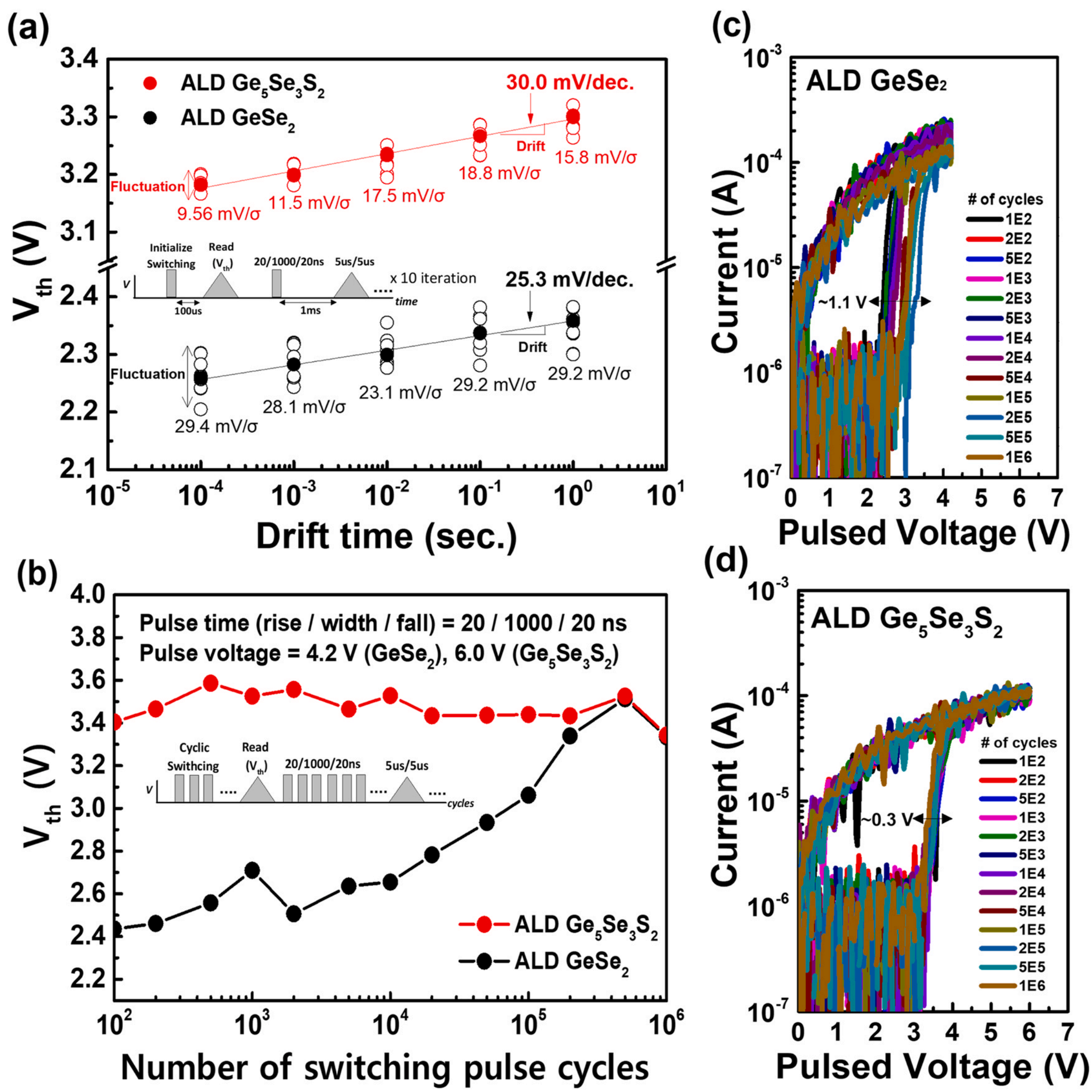

Fig. 5. (a) V_{th} drift and V_{th} fluctuation characteristics of 10-nm-thick ALD $GeSe_2$ and $Ge_5Se_3S_2$ OTS devices; (b) V_{th} fluctuation with endurance cycles; (c, d) Pulse I–V curves with endurance cycles.

X-point arrays [33]. Because the E_g of amorphous chalcogenide corresponds to the activation energy (E_a) of the modified Poole--Frenkel (PF) equation by the trap-limited conduction model, which describes the electrical conduction mechanism of OTS, the OTS materials with a high E_g are reported to have a low I_{off} and high E_{th} [34,35]. In the Tauc plot shown in Fig. S5, it was confirmed that the E_g extracted as a linear trend line when $(\alpha h\upsilon)^{1/2}$ is zero was 1.15 and 1.35 eV for the ALD $GeSe_2$ and ALD $Ge_5Se_3S_2$, respectively. The reason $Ge_5Se_3S_2$ has a high E_g is that although the proportion of Group 6 chalcogen elements (i.e., S, Se, Te) is small, the E_g contribution of S is greater than that of Se [36,37]. In addition, Tauc parameters ($B^{1/2}$), which is the slope of tangent line of Tauc plot, were extracted to obtain information for the film disorder [38,39]. Extracted Tauc parameters of $GeSe_2$ and $Ge_5Se_3S_2$ showed similar values of 586.6 and 591.4 $cm^{-1/2}eV^{-1/2}$, respectively, and this means that post sulfurization process in this work didn't significantly affect the film disorder of $GeSe_2$.

3.5. AC characteristics

Fig. 4(e, f) show the time-dependent I–V curve, from which V_{th} can be extracted using triangular pulses (rising/falling = 5 μs/5 μs) for reliability evaluation. Both ALD $GeSe_2$ and ALD $Ge_5Se_3S_2$ showed on-current characteristics of 100 μA or more, and switching characteristics were confirmed at a level similar to V_{th}, shown in the DC I–V curves in Fig. 4(c, d). Also, both devices were turned on within 75 ns as shown Figs. S6. The OTS devices with ALD $GeSe_2$ and $Ge_5Se_3S_2$ investigated the V_{FF}, V_{th}, I_{off}, and I_{on} characteristics as the basic requirements of the selector of the 3D X-point memory architecture. Next, reliability characteristics were explored.

Fig. 5(a) shows the V_{th} drift characteristics, which are popular as a mechanism of defect annihilation by structure relaxation of amorphous chalcogenides over time [40]. In addition, the V_{th} fluctuation related to random telegraph noise (RTN) caused by electron capture and emission at a trap site were analyzed together through repeated V_{th} drift measurements [41]. The read window margin (RWM) of 3D X-point memory suffers as the values of these two parameters increase [41]. For the median characteristics of the ALD $GeSe_2$ devices, the V_{th} drift was 25.3 mV/decade and the V_{th} fluctuation was 27.8 mV/σ. In contrast, for ALD $Ge_5Se_3S_2$ devices, the median values of V_{th} drift and V_{th} fluctuation were 30.0 mV/decade and 14.6 mV/σ, respectively. ALD $Ge_5Se_3S_2$ showed a slight increase in the V_{th} drift but a significant decrease in the V_{th} fluctuation compared to ALD $GeSe_2$. Fig. 5(b–d) show the cyclic switching

Table 1
Summary of OTS device`s median characteristics of 10-nm-thick ALD $GeSe_2$ and $Ge_5Se_3S_2$.

	$GeSe_2$	$Ge_5Se_3S_2$
V_{ff}	**3.4 V**	**4.3 V**
V_{th}	**1.9 V**	**3.2 V**
$I_{off,1/2}$	**200 nA**	**40 nA**
V_{th} drift	**25.3 mV/dec.**	**30.0 mV/dec.**
STVF	**27.8 mV/σ**	**14.6 mV/σ**
LTVF	**1.1 V**	**0.3 V**
Endurance	**> 10^6 cyc.**	**> 10^6 cyc.**

* * STVF = Short-Term V_{th} Fluctuation
* * LTVF = Long-Term V_{th} Fluctuation

endurance characteristics of the ALD $GeSe_2$ and $Ge_5Se_3S_2$. The cyclic switching pulses of the two devices were applied at 4.2 and 6.0 V, respectively, considering the V_{th} difference and the normalized on-state current of approximately 100 µA. In both cases, hard failures did not occur until 10^6 cycles. However, the ALD $GeSe_2$ showed a large increasing directional long-term V_{th} fluctuation of approximately 1.1 V in the long cyclic switching operation, whereas the ALD $Ge_5Se_3S_2$ showed a monotonous small long-term V_{th} fluctuation of approximately 0.3 V. ALD $GeSe_2$ is likely to be seen as a soft failure, depending on the read and write operation margins of the 3D X-point memory.

The difference in the V_{th} drift and V_{th} fluctuation characteristics between ALD $GeSe_2$ and $Ge_5Se_3S_2$ can be attributed to the ratio of Ge and chalcogen elements (S, Se). Because $Ge_5Se_3S_2$ is rich in thermodynamically unfavorable Ge-Ge bonds, it can be explained that the V_{th} drift is larger owing to the relaxation and aging of Ge-Ge bonds with time [42]. Meanwhile, for the ALD $GeSe_2$, non-preferred Ge-Ge bonds are generated and activated at longer cyclic switching operations, unlike the ALD $Ge_5Se_3S_2$ with a large number of Ge-Ge bonds that already exist [43]. Unlike the binary Ge-rich Ge_xSe_{1-x}, the ternary $Ge_5Se_3S_2$ replaced Se with shorter bond-length atoms of S, and moved toward stronger and shorter bonds, resulting in larger hybridization parameters [8]. Furthermore, statistical distribution in mobility gap-induced repetitive switching can be expected to decrease because the ratio of chalcogen acting as deep trap sites is reduced [44]. The design of the OTS material replacing Se with S while reducing the proportion of chalcogen revealed that it maintains a more stable amorphous state with small V_{th} fluctuations.

4. Conclusions

We studied the process and device characteristics of novel ternary Ge-Se-S for OTS applications. DFT calculation was utilized to predict feasibility of the ALD reaction with $HGeCl_3$ and $Se(SiMe_3)_2$. Based on DFT result, ALD $GeSe_2$ thin films were synthesized using $HGeCl_3$ and $Se(SiMe_3)_2$ precursors. By controlling the temperature and time of the post plasma sulfurization process, composition of $GeSe_2$ was controlled from $GeSe_2$ to Ge_2S. It was confirmed that excellent step-coverage and amorphous phase of $GeSe_2$ were maintained after the post sulfurization process. Finally, we fabricated OTS devices with a 50-nm BEC using 10-nm-thick ALD $GeSe_2$ and $Ge_5Se_3S_2$ and investigated the DC characteristics, reliability of the V_{th} drift, fluctuation, and endurance. The OTS device of ALD $Ge_5Se_3S_2$ showed higher V_{th} (3.2 V), lower $I_{off,1/2}$ (~40 nA), smaller short-term V_{th} fluctuation (14.6 mV/σ), and more stable long-term V_{th} fluctuation (< ~0.3 V up to 10^6 cycles) although V_{th} drift (~30.0 mV/decade) increased slightly compared to ALD $GeSe_2$ as shown in Table 1. This study on the ALD ternary $Ge_5Se_3S_2$ will contribute to the preparation of future 3D X-point memory scaling.

CRediT authorship contribution statement

Sukhwan Jun: Conceptualization, Data curation, Formal analysis, Investigation, Methodology, Resources, Validation, Writing - original draft, Writing - review & editing. **Seunggi Seo**: Software, Methodology. **Seungwon Park**: Data curation, Formal analysis. **Tae Hyun Kim**: Formal analysis, Methodology. **Minkyu Lee**: Data curation. **Seok Man Hong**: Formal analysis. **Taehoon Kim**: Funding acquisition, Investigation. **Seung-min Chung**: Writing - review & editing. **Taeyoon Lee**: Funding acquisition, Data curation. **Myoungsub Kim**: Methodology, Project administration, Supervision. **Hyungjun Kim**: Funding acquisition, Project administration, Supervision.

Data availability

The data that has been used is confidential.

Declaration of Competing Interest

The authors declare that they have no known competing financial interests or personal relationships that could have appeared to influence the work reported in this paper.

Acknowledgments

This study was the result of a research project supported by SK hynix Inc. This work was supported by the National Supercomputing Center with supercomputing resources including technical support (KSC-2021-CRE-0561). This work was supported by Priority Research Centers Program through the National Research Foundation of Korea (NRF-2019R1A6A1A11055660). We would also like to thank Merck for providing Ge and Se precursors.

Appendix A. Supporting information

Supplementary data associated with this article can be found in the online version at doi:10.1016/j.jallcom.2023.169514.

References

[1] S.R. Ovshinsky, Reversible electrical switching phenomena in disordered structures, Phys. Rev. Lett. 21 (1968) 1450–1453, https://doi.org/10.1103/PhysRevLett.21.1450
[2] A. Chen, Emerging memory selector devices, 13th Non-Volatile Memory Technology Symposium, NVMTS 2013. 2013. https://doi.org/10.1109/NVMTS.2013.6851049.
[3] J. Woo, X. Peng, S. Yu, Design Considerations of Selector Device in Cross-Point RRAM Array for Neuromorphic Computing, Proceedings - IEEE International Symposium on Circuits and Systems. 2018–2 2018. https://doi.org/10.1109/ISCAS.2018.8351735.
[4] D.C. Kau, The pursuit of atomistic switching and cross point memory, VLSI-TSA 2021 - 2021 International Symposium on VLSI Technology, Systems and Applications, Proceedings. 2021. https://doi.org/10.1109/VLSI-TSA51926.2021.9440112.
[5] Y. Huai, H. Yang, X. Hao, Z. Wang, R. Malmhall, K. Sato, J. Zhang, D.H. Jung, X. Wang, P. Xu, B.K. Yen, High Density 3D Cross-Point STT-MRAM, In: Proceedings of the 2018 IEEE 10th International Memory Workshop, IMW 2018. (2018) 1–4. https://doi.org/10.1109/IMW.2018.8388833.
[6] J.M. Lopez, D.A. Robayo, L. Grenouillet, C. Carabasse, G. Navarro, R. Fournel, C. Sabbione, M. Bernard, O. Billoint, C. Cagli, L. Couture, D. Deleruyelle, M. Bocquet, J.M. Portal, E. Nowak, G. Molas, Optimization of RRAM and OTS selector for advanced low voltage CMOS compatibility, In: 2020 IEEE International Memory Workshop, IMW 2020 - Proceedings, Institute of Electrical and Electronics Engineers Inc., 2020. https://doi.org/10.1109/IMW48823.2020.9108126.
[7] N. Gong, W. Chien, Y. Chou, C. Yeh, N. Li, H. Cheng, C. Cheng, I. Kuo, C. Yang, R. Bruce, A. Ray, L. Gignac, Y. Lin, C. Miller, T. Perri, W. Kim, L. Buzi, H. Utomo, F. Carta, E. Lai, H. Ho, H. Lung, M. Brightsky, A no-verification multi-level-cell (MLC) operation in cross-point OTS-PCM, (2020) 60–61.
[8] H. Li, J. Robertson, Materials selection and mechanism of non-linear conduction in chalcogenide selector devices, Sci. Rep. 9 (2019) 1–9, https://doi.org/10.1038/s41598-018-37717-x

[9] Youngjun Kim Myoungsub Kim, S. Minkyu Lee, H.Keun Man Hong, Sijung Kim, Taehoon Yoo, Seung-min Kim, Taeyoon Chung, Hyungjun Lee, Kim, PE-ALD of Ge 1−x S x amorphous chalcogenide alloys for OTS applications, J. Mater. Chem. C. Mater. 9 (2021) 6006–6013, https://doi.org/10.1039/D1TC00650A

[10] P. Noé, A. Verdy, F. Acapito, J. Dory, M. Bernard, G. Navarro, J. Jager, J. Gaudin, J. Raty, Toward ultimate nonvolatile resistive memories: the mechanism behind ovonic threshold switching revealed, Sci. Adv. 70 (2020) 1–11.

[11] S. Jia, H. Li, T. Gotoh, C. Longeaud, B. Zhang, J. Lyu, S. Lv, M. Zhu, Z. Song, Q. Liu, J. Robertson, M. Liu, Ultrahigh drive current and large selectivity in GeS selector, Nat. Commun. 11 (2020) 1–9, https://doi.org/10.1038/s41467-020-18382-z

[12] Y.K. Lee, C. Yoo, W. Kim, J.W. Jeon, C.S. Hwang, Atomic layer deposition of chalcogenides for next-generation phase change memory, J. Mater. Chem. C. Mater. 9 (2021) 3708–3725, https://doi.org/10.1039/d1tc00186h

[13] V. Adinolfi, M. Laudato, R. Clarke, V.K. Narasimhan, L. Cheng, K. Littau, Atomic layer deposition of germanium-selenium-tellurium compounds for low-leakage, tunable ovonic threshold switches, J. Vac. Sci. Technol. A 38 (2020) 052404, https://doi.org/10.1116/6.0000285

[14] C. Yoo, W. Kim, J.W. Jeon, E.-S. Park, M. Ha, Y.K. Lee, C.S. Hwang, Atomic layer deposition of GexSe1−x thin films for endurable ovonic threshold selectors with a low threshold voltage, ACS Appl. Mater. Interfaces 12 (2020) 23110–23118, https://doi.org/10.1021/ACSAMI.0C03747

[15] A. Haider, S. Deng, W. Devulder, J.W. Maes, J.-M. Girard, G. Khalil El Hajjam, G.S. Kar, K. Opsomer, C. Detavernier, M. Givens, L. Goux, S. Van Elshocht, R. Delhougne, A. Delabie, M. Caymax, J. Swerts, Pulsed chemical vapor deposition of conformal GeSe for application as an OTS selector, Mater. Adv. 2 (2021) 1635–1643, https://doi.org/10.1039/d0ma01014f

[16] W. Kim, S. Yoo, C. Yoo, E.S. Park, J. Jeon, Y.J. Kwon, K.S. Woo, H.J. Kim, Y.K. Lee, C.S. Hwang, Atomic layer deposition of GeSe films using HGeCl3 and [(CH3)3Si] 2Se with the discrete feeding method for the ovonic threshold switch, Nanotechnology 29 (2018) 365202, https://doi.org/10.1088/1361-6528/aacda0

[17] V. Adinolfi, L. Cheng, M. Laudato, R.C. Clarke, V.K. Narasimhan, S. Balatti, S. Hoang, K.A. Littau, Composition-controlled atomic layer deposition of phase-change memories and ovonic threshold switches with high performance, ACS Nano 13 (2019) 10440–10447, https://doi.org/10.1021/acsnano.9b04233

[18] V. Adinolfi, M. Laudato, R. Clarke, V.K. Narasimhan, L. Cheng, K. Littau, Atomic layer deposition of germanium-selenium-tellurium compounds for low-leakage, tunable ovonic threshold switches, J. Vac. Sci. Technol. A 38 (2020) 052404, https://doi.org/10.1116/6.0000285

[19] P. Noé, A. Verdy, F. D′acapito, J.-B. Dory, M. Bernard, G. Navarro, J.-B. Jager, J. Gaudin, J.-Y. Raty, Toward ultimate nonvolatile resistive memories: The mechanism behind ovonic threshold switching revealed, 2020. https://www.science.org.

[20] A. Verdy, G. Navarro, M. Bernard, S. Chevalliez, N. Castellani, E. Nolot, J. Garrione, P. Noe, G. Bourgeois, V. Sousa, M.C. Cyrille, E. Nowak, Carbon electrode for Ge-Se-Sb based OTS selector for ultra low leakage current and outstanding endurance, In: IEEE International Reliability Physics Symposium Proceedings, Institute of Electrical and Electronics Engineers Inc., 2018: pp. 6D.41–6D.46. https://doi.org/10.1109/IRPS.2018.8353635.

[21] Oyō Butsuri Gakkai, IEEE electron devices society, In: Proceedings of the 2018 IEEE Symposium on VLSI Technology: 18–22 June 2018., n.d.

[22] G.P. and H.N.W.C. M. Frisch, G. Trucks, H. Schlegel, G. Scuseria, M. Robb, J. Cheeseman, G. Scalmani, V. Barone, Gaussian 16, Gaussian Inc, (2016).

[23] A.D. Becke, Densityfunctional thermochemistry. III. The role of exact exchange Density-functional thermochemistry. III. The role of exact exchange, J. Chem. Phys. 98 (1993) 5648, https://doi.org/10.1063/1.464913

[24] C. Lee, W. Yang, R.G. Parr, Development of the Colle-Salvetti correlation-energy formula into a functional of the electron density, Phys. Rev. B 37 (1988) 785, https://doi.org/10.1103/PhysRevB.37.785

[25] S. Grimme, S. Ehrlich, L. Goerigk, Effect of the damping function in dispersion corrected density functional theory, J. Comput. Chem. 32 (2011) 1456–1465, https://doi.org/10.1002/JCC.21759

[26] S. Grimme, J. Antony, S. Ehrlich, H. Krieg, A consistent and accurate ab initio parametrization of density functional dispersion correction (DFT-D) for the 94 elements H-Pu, J. Chem. Phys. 132 (2010) 154104, https://doi.org/10.1063/1.3382344

[27] B. Han, Y.J. Kim, J.M. Park, L.L. Yusup, J. Shin, W.J. Lee, Reaction mechanism for atomic layer deposition of germanium ditelluride thin films, J. Nanosci. Nanotechnol. 17 (2017), https://doi.org/10.1166/jnn.2017.14044

[28] S. Seo, W.J. Woo, Y. Lee, H. Yoon, M. Kim, I.K. Oh, S.M. Chung, H. Kim, B. Shong, Reaction mechanisms of non-hydrolytic atomic layer deposition of Al2O3 with a series of alcohol oxidants, J. Phys. Chem. C 125 (2021) 18151–18160, https://doi.org/10.1021/acs.jpcc.1c03518

[29] K.Y. Ko, S. Lee, K. Park, Y. Kim, W.J. Woo, D. Kim, J.G. Song, J. Park, J.H. Kim, Z. Lee, H. Kim, High-performance gas sensor using a large-area WS2 xSe2-2 x alloy for low-power operation wearable applications, ACS Appl. Mater. Interfaces 10 (2018) 34163–34171, https://doi.org/10.1021/acsami.8b10455

[30] D. Sahoo, S. Sahoo, D. Alagarasan, R. Ganesan, S. Varadharajaperumal, R. Naik, Proton ion irradiation on As40Se50Sb10 thin films: fluence-dependent tuning of linear-nonlinear optical properties for photonic applications, ACS Appl. Electron Mater. 4 (2022) 856–868, https://doi.org/10.1021/acsaelm.1c01223

[31] A. Verdy, G. Navarro, M. Bernard, S. Chevalliez, N. Castellani, E. Nolot, J. Garrione, P. Noe, G. Bourgeois, V. Sousa, M.C. Cyrille, E. Nowak, Carbon electrode for Ge-Se-Sb based OTS selector for ultra low leakage current and outstanding endurance, IEEE International Reliability Physics Symposium Proceedings. 2018-March (2018) 6D.41–6D.46. https://doi.org/10.1109/IRPS.2018.8353635.

[32] S.Y. Shin, J.M. Choi, J. Seo, H.W. Ahn, Y.G. Choi, B.K. Cheong, S. Lee, The effect of doping Sb on the electronic structure and the device characteristics of ovonic threshold switches based on Ge-Se, Sci. Rep. 4 (2014), https://doi.org/10.1038/srep07099

[33] N.S. Avasarala, G.L. Donadio, T. Witters, K. Opsomer, B. Govoreanu, A. Fantini, S. Clima, H. Oh, S. Kundu, W. Devulder, M.H. Van Der Veen, J. Van Houdt, M. Heyns, L. Goux, G.S. Kar, Half-threshold bias Ioff reduction down to nA range of thermally and electrically stable high-performance integrated OTS selector, obtained by Se enrichment and N-doping of thin GeSe layers, Digest of Technical Papers - Symposium on VLSI Technology. 2018-June (2018) 209–210. https://doi.org/10.1109/VLSIT.2018.8510680.

[34] D. Ielmini, Y. Zhang, Analytical model for subthreshold conduction and threshold switching in chalcogenide-based memory devices, J. Appl. Phys. 102 (2007), https://doi.org/10.1063/1.2773688

[35] T. Kim, D. Lee, J. Kim, H. Sohn, Trap-controlled space-charge-limited conduction in amorphous As x Te1-x thin films with ovonic threshold switching, Appl. Phys. Express 13 (2020), https://doi.org/10.35848/1882-0786/ab827c

[36] S. Kasap, P. Capper (Eds.), Springer Handbook of Electronic and Photonic Materials, Springer, 2017, https://doi.org/10.1007/978–3-319–48933-9

[37] M. Dongol, A.F. Elhady, M.S. Ebied, A.A. Abuelwafa, Impact of sulfur content on structural and optical properties of Ge20Se80−xSx chalcogenide glasses thin films, Opt. Mater. 78 (2018) 266–272, https://doi.org/10.1016/j.optmat.2018.02.033

[38] R. Naik, R. Ganesan, K.S. Sangunni, Optical properties change with the addition and diffusion of Bi to As 2S3 in the Bi/As2S3 bilayer thin film, J. Alloy. Compd. 554 (2013) 293–298, https://doi.org/10.1016/j.jallcom.2012.11.198

[39] R. Naik, R. Ganesan, K.S. Sangunni, Photo induced optical changes in Sb/As2S3 multilayered film and (As2S3)0.93Sb 0.07 film of equal thickness, J. Alloy. Compd. 505 (2010) 249–254, https://doi.org/10.1016/j.jallcom.2010.06.039

[40] D. Ielmini, D. Sharma, S. Lavizzari, A.L. Lacaita, Reliability impact of chalcogenide-structure relaxation in phase-change memory (PCM) cells-Part I: experimental study, IEEE Trans. Electron Devices 56 (2009) 1070–1077, https://doi.org/10.1109/TED.2009.2016397

[41] T. Kim, S. Lee, Evolution of phase-change memory for the storage-class memory and beyond, IEEE Trans. Electron Devices 1 (2020) 1–13, https://doi.org/10.1109/ted.2020.2964640

[42] S. Clima, D. Garbin, W. Devulder, J. Keukelier, K. Opsomer, L. Goux, G.S. Kar, G. Pourtois, Material relaxation in chalcogenide OTS SELECTOR materials, Micro Eng. 215 (2019) 110996, https://doi.org/10.1016/J.MEE.2019.110996

[43] Z. Chai, W. Zhang, S. Clima, F. Hatem, R. Degraeve, Q. Diao, J.F. Zhang, P. Freitas, J. Marsland, A. Fantini, D. Garbin, L. Goux, G.S. Kar, Cycling induced metastable degradation in GeSe ovonic threshold switching selector, IEEE Electron Device Lett. 42 (2021) 1448–1451, https://doi.org/10.1109/LED.2021.3109582

[44] S. Clima, D. Garbin, K. Opsomer, N.S. Avasarala, W. Devulder, I. Shlyakhov, J. Keukelier, G.L. Donadio, T. Witters, S. Kundu, B. Govoreanu, L. Goux, C. Detavernier, V. Afanas'ev, G.S. Kar, G. Pourtois, Ovonic threshold-switching GexSey chalcogenide materials: stoichiometry, trap nature, and material relaxation from first principles, Phys. Status Solidi (RRL) – Rapid Res. Lett. 14 (2020) 1900672, https://doi.org/10.1002/PSSR.201900672